Fine structure of the atomic scattering factors near the iridium *L*-edges

Hisamitsu Awaki,[a,*] Yoshitomo Maeda,[b] Hironori Matsumoto,[c] Marcos Bavdaz,[d] Finn E. Christensen,[e] Maximilien Collon,[f] Desiree D. M. Ferreira,[e] Kazunori Ishibashi,[g] Sonny Massahi,[e] Takuya Miyazawa,[h] Sara Svendsen,[e] and Keisuke Tamura[i]

[a]Ehime University, Faculty of Science, Matsuyama, Japan
[b]ISAS/JAXA, Sagamihara, Japan
[c]Osaka University, Graduate School of Science, Toyonaka, Japan
[d]European Space Research and Technology Centre, Noordwijk, The Netherlands
[e]Technical University of Denmark, DTU Space, National Space Institute, Lyngby, Denmark
[f]cosine, Warmond, The Netherlands
[g]Nagoya University, Graduate School of Science, Nagoya, Japan
[h]Okinawa Institute of Science and Technology Graduate University, Okinawa, Japan
[i]Maryland University Center for Space Science Technology, Baltimore, Maryland, United States

Abstract We measured the reflectivity of an Athena silicon pore optics sample coated with 10-nm thick iridium near the iridium L-edges (L_3, L_2, and L_1) in a step of 1.5 eV. The derived atomic scattering factor f_2 was similar to a shape of the absorption coefficient μ near L_3 and L_2 obtained by previous x-ray absorption spectroscopy (XAS) measurements. The fine structures of f_2 of L_3 and L_2 can be represented by a strong sharp line referred to as a white line (WL) and two weak lines at center energies of ∼17 and ∼31 eV from each edge energy. The branching ratio (L_3/L_2) of the WL is >2, which reflects the initial core-electron states available for the L_2 ($2p_{1/2}$) and L_3 ($2p_{3/2}$) processes, and the ratio remains high to the energy of +7.5 eV from WL. The fine structure seen in L_1 also has two weak lines, which were seen in XAS at L_1-edge. Our measurements near L_3, L_2, and L_1 edges demonstrated a different technique to provide atomic structural information as XAS. The ground calibration to measure fine structures near the edges may potentially be simplified using f_2 estimated based on μ. [DOI: 10.1117/1.JATIS.8.4.044001]

Keywords: atomic scattering factors; iridium; x-ray absorption near edge structure; x-ray absorption fine structure.

Paper 22059G received Jun. 9, 2022; accepted for publication Sep. 26, 2022; published online Oct. 22, 2022.

1 Introduction

The x-ray absorption fine structure (XAFS) is often measured with x-ray absorption spectroscopy (XAS) to find useful information on the environment (geometry) and electronic structure of the absorbing atoms. XAS is performed in a transmission setup, providing a direct measure of the linear x-ray attenuation coefficient $\mu(E)$. The x-ray absorption edge spectra of iridium, which is one of the elements having high electron density, such as Au, Pt, etc., have been obtained to reveal the fundamental characteristics of the 5*d* material[1–3]. Clancy et al.[1] (hereafter Clancy12) investigated spin-orbit coupling effects in a series of Ir- and Re-based 5*d* compounds using XAS techniques and observed anomalously large L_3/L_2 branching ratios in all Ir-based compounds, indicating a very large expectation value for the spin-orbit operator in these systems.

On the other hand, small oscillations are seen in the reflectance setup, referred to as the diffraction anomalous fine structure (DAFS). Stragier et al.[4] studied the DAFS as a new x-ray

*Address all correspondence to Hisamitsu Awaki, awaki@astro.phys.sci.ehime-u.ac.jp

structural technique and demonstrated that the DAFS measurements provide the same local atomic structural information as XAFS. They used XAFS standards to analyze the DAFS data by shifting the phase. Pickering et al.[5] applied the Kramers–Kronig relation to the atomic scattering factors f_1 and f_2 and determined the scattering factor f_2 to fit the DAFS data. The scattering factor f_2 is suitable for research of XAFS because f_2 is related to the absorption coefficient μ: $f_2 = \pi/2\ CE\mu$,[6] where $C = (\pi r_0 hc)^{-1}$, h is the Planck's constant, r_0 is the classical electron radius, and c is the speed of light. However, the f_1 value in the wide energy band is required for calculating the f_2 value using the Kramers–Kronig relation.

The atomic scattering factors f_1 and f_2 of iridium can be derived from the reflectance obtained by angular scan and/or energy scan without using the Kramers–Kronig relation. This is demonstrated by measurements on the ground for building the response function of the x-ray mirror (e.g., ASTRO-H[7] and Chandra[8]). We measured the reflectance of a sample fabricated by employing ESAs silicon pore optics (SPO) technology in the high energy region from 9000 to 15,000 eV at the synchrotron radiation facility SPring-8[9] and obtained the atomic scattering factors of iridium near L-edges with an energy pitch of 1.5 eV. We compare the f_2 fine structure with XAFS and show that the method using reflection is as effective as XAFS methods. In addition, it is becoming increasingly important to measure the fine structure of the atomic scattering factors because of the improvement in energy resolution of focal plane detectors in recent years.[10,11] Although fine energy scans for measuring f_1 and f_2 near the edges are possible, estimating f_2 from μ can reduce the time required for ground calibration tests.[7,9]

In Sec. 2, we introduce our x-ray measurements and calculate the atomic scattering factors from the reflectance. In Sec. 3, we characterize the fine structure seen in the atomic scattering factor f_2 to compare the previous work on XAFS and then analyze the derived f_2 in a way similar to XAS.

2 X-Ray Measurement and Estimation of the Atomic Scattering Factors

2.1 *X-Ray Measurement*

Our SPO sample was prepared at the coating facility dedicated for the Athena mirror production.[12,13] The sample has a length and width of 110 and 49 mm, respectively. A 10-nm thick iridium thin film coating was deposited using DC magnetron sputtering. The details of the sample preparation are described in Awaki et al. 2021.[9]

We measured the x-ray reflectivity of the SPO sample at BL20B2[14] in SPring-8. The crystal plane of 311 of the Si double crystal monochromator[15] was selected to monochromatize continuum x-rays in our experiment. The energy resolution ($\Delta E/E$) of the available x-ray beam is $<10^{-4}$ in the energy range from 9000 to 15,000 eV, and the energy scale was calibrated by measurements of the Cu K-edge structure. We measured the intensity of a reflected x-ray on the SPO sample as well as the intensity of an incident x-ray and derived the reflectance R, defined as the ratio of the intensity of a reflected x-ray to that of the incident x-rays. Since the reflectance R is described as a function of the energy E of the incident x-ray and grazing angle θ, we measured the reflectivity by performing angle and energy scans at fixed energies and fixed incident angles, respectively.

In the energy scans, three fine pitch scans with an incident angle of 0.2, 0.32, and 0.4 deg were performed around the energies of the iridium L-edges in steps of 1.5 eV to clarify the iridium L-shell structure of f_1 and f_2. The scanning energy ranges are 11 to 11.5 keV for L_3 edge, 12.5 to 13 keV for L_2 edge, and 13.2 to 13.7 keV for L_1 edge. Figure 1 shows the reflectance obtained in the energy scans. We can clearly see small oscillations in the post-edge region. These small oscillations are referred to as DAFS. Angle scans were performed at x-ray energies of 11, 12, and 14 keV, spanning the range of the iridium L-edges, specifically. The incident angle was scanned up to 1.5 deg in steps of 0.05 deg to measure the thickness of the iridium layer.

2.2 *Estimation of the Atomic Scattering Factors*

The reflectance of a single thin layer can be calculated using the refractive indices of the thin layer and the substrate. By fitting the measured data with a single thin layer model, we can estimate the parameters describing the iridium layer, specifically, the thickness of the iridium

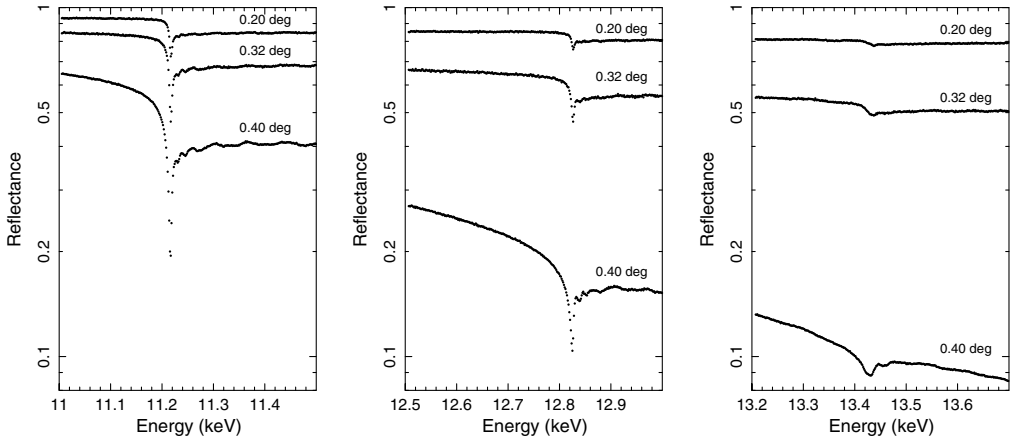

Fig. 1 Iridium *L*-edge structure of the reflectance obtained by the energy scan in steps of 1.5 eV.

layer (d), interfacial roughness between the iridium layer and SPO substrate (σ_b), and the surface roughness of the iridium layer (σ). However, the angle data points in the energy scan were not enough to estimate the parameters. Thus, the fit to the angle scan data was used to identify the parameters describing the iridium layer, specifically, d, σ_b, and σ. In this calculation, the loss of reflectance owing to roughness was considered as the Nevot–Croce factor,[16] and the atomic weight and the corresponding mass density of iridium were taken as 192.22 and 22.421 g cm^{-3},[17] respectively. We employed an overlayer model, assumed as a hydrocarbon chain of the form CH_2 with a density of 1 g/cm^3 (Graessle et al.[8]). The best-fit values were obtained from the angle scan. The details of the measurements are given in Awaki et al.[9]

In the fitting procedure of the energy scan data, σ, σ_b, and d were set as constant at the weighted mean values of the best-fit values of the angle scan data ($\sigma = 0.30$ nm, $\sigma_b = 0.64$ nm, $d = 10.01$ nm). The thicknesses of the overlayer were set to be 0.9 nm because we found that an overlayer thickness of 0.9 nm led to a better fit to the f_2 data reported by Henke et al.[6] Figure 2 shows the derived f_2 near the iridium L-edges to clarify their structures.

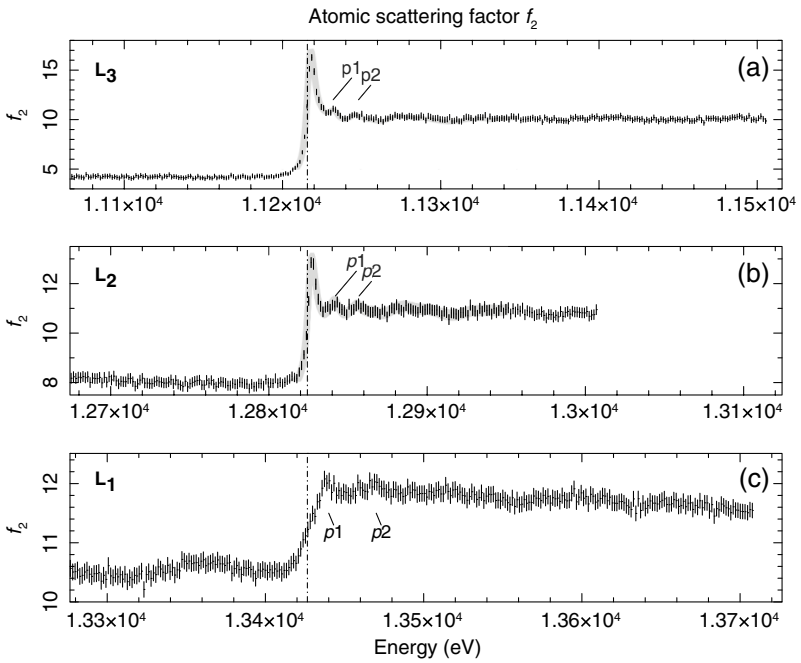

Fig. 2 The atomic scattering factor f_2 near the L-edges. The dash-dotted lines indicate the energies (11215.7 ±0.3 eV, 12824.3 ±0.9 eV, and 13426.5 ±0.6 eV) of L_3, L_2, and L_1 edges, respectively.[9] The gray line in the panels of L_2 and L_3 shows $\mu(E)$ (arb. unit) obtained by Clancy12.

Table 1 L_3 and L_2 white lines.

	Awaki+21	Monteseguro+19	Clancy12
L_3 WL			
Center energy (eV)	11217.9 ± 0.2	11217.4 ± 0.2	11218.1 ± 0.1
Width (eV)	6.7 ± 0.4	6.9 ± 0.2	6.6 ± 0.1
Integrated intensity[a]	21.9 ± 1.0	13.5 ± 0.9	14.3 ± 0.6
L_2 WL			
Center energy (eV)	12827.3 ± 0.3	N/A	
Width (eV)	4.6 ± 0.8	N/A	
Integrated intensity[a]	8.4 ± 0.9	N/A	
Branching ratio[b]	2.6 ± 0.4	N/A	3.2 ± 0.1

Error ranges represent 1σ confidence boundaries for the parameter of interest ($\chi^2_{\mathrm{min}} + 1$).
[a]Our result is estimated from f_2, while Monreseguro et al.[20] and Clancy12 estimated the parameters from μ.
[b]The branching ratio is changed to 2.9 ± 0.4, if the line width of L_2 WL is fixed to the same line width as L_3 WL.

3 Fine Structures Derived from the Atomic Scattering Factor f_2

3.1 *Comparison with the XANES Obtained from XAS*

It is known that the absorption coefficient $\mu(E)$ of iridium near L_2 and L_3 edges contains three main features: (i) a sharp line feature known as "white line"[18,19] (hereafter WL), (ii) a step-like edge feature, and (iii) a small wave-like feature.[1,20] The scattering factor f_2 near L_2 and L_3 edges also shows these features (see Fig. 2). To confirm the similarity between $\mu(E)$ by Clancy12 and our result $f_2(E)$, the Clancy12 data (arb. unit) was scaled to fit our data and then overlaid on our data in Fig. 2. Both data were found to be similar, including the small wave feature in the energy $\Delta E > 50$ eV. The similarity suggests that (1) the fine structures of f_2 obtained from reflectance are consistent with XAFS obtained from XAS and (2) there is no apparent difference of optical characteristics between a thin iridium film formed by a DC magnetron sputter and an iridium powder with a purity of 99.99%.

The similarity to Clancy12 can also be seen in the best-fit parameters of $L3$. Comparing the best-fit parameters obtained by Awaki et al.[9] with previous works,[1,20] the best-fit parameters (center energy and line width) of $L3$ WL were consistent with previous works[1,20] (see Table 1). Clancy12 also measured L_2 WL and estimated the branching ratio to be 3.2, which is larger than that of our result. In the fitting procedure by Clancy12, the line width of L_2 WL was fixed to the same line width as L_3 WL. Thus, we fitted the L_2 WL with the same line width as L_3 WL. The branching ratio is changed to 2.9 ± 0.4, which is consistent with their result.

3.2 *Fine Structures of the Scattering Factor* f_2 *Near L-Edges*

There are two distinct peaks ($p1$ and $p2$ in Fig. 2) in the f_2 fine structures at L_2 and L_3-edges, and these peaks are also seen in the x-ray absorption near edge structure (XANES) results obtained by previous works.[1] Each peak was fitted with a Lorentzian model. The best-fit parameters are shown in Table 2. The center energy of each peak is represented by the energy ΔE from the absorption edge. Since the center energies ΔE and line widths of $p1$ in the L_3 edge are consistent with those of $p1$ in L_2 edge in the 1σ error region, p1 detected in L_2 edge is considered to be a transition to the same state as detected at L_3 edge. It would be the same for $p2$ as for $p1$. Sham[21] studied the x-ray absorption fine structures at L-edges for 4d elements, Rh, Pd, and Ag, and there were prominent weak peaks at $\tilde{2}0$ and $\sim$38 eV in their absorption spectrum at the L-edge for these materials. The two weak lines $p1$ and $p2$ in Fig. 2 would be assigned to peaks 2 to 4 ($\rightarrow pd$) and 5 ($\rightarrow df$) in Table 1 of Sham.[21] To find branching ratios of these lines,

Table 2 Best fit parameters of two peaks in *L*-edge structure.

	L_3 (11215.7 ± 0.3a)	L_2 (12824.3 ± 0.9a)	L_1 (13426.5 ± 0.6a)
First peak ($p1$)			
ΔE (eV)[b]	17.1 ± 0.6	$18.0^{+1.3}_{-2.0}$	$12.2^{+1.1}_{-0.9}$
Width (eV)	$3.7^{+2.2}_{-1.7}$	$5.3^{+7.5}_{-4.0}$	$6.6^{+3.8}_{-2.6}$
Integrated intensity	$2.7^{+1.1}_{-0.7}$	$1.0^{+1.1}_{-0.5}$	1.1 ± 0.3
Second peak ($p2$)			
ΔE (eV)[b]	$30.9^{+2.4}_{-1.6}$	$32.2^{+2.0}_{-1.0}$	$42.0^{+2.3}_{-3.3}$
Width (eV)	$6.1^{+6.4}_{-3.8}$	$5.5^{+8.2}_{-4.2}$	11^{+16}_{-6}
Integrated intensity	$1.2^{+.08}_{-0.5}$	$0.9^{+1.5}_{-0.5}$	0.6 ± 0.3
WL			
ΔE (eV)[b]	2.3 ± 0.1	3.0 ± 0.2	N/A

Error ranges represent 1σ confidence boundaries for a parameter of interest ($\chi^2_{\min} + 1$).
[a]Edge energy in units of eV. These values are quoted from Awaki et al.[9]
[b]ΔE is the energy from the absorption edge.

we fixed both the center energies and the line width (Γ_E) of the two peaks at the weighted mean values ($\Delta E = 17.1$ and 31.8 eV, $\Gamma_E = 3.9$ and 4.6 eV for $p1$ and $p2$, respectively) and fitted $p1$ and $p2$ with a Lorentzian model. The branching ratio of $p1$ was larger than 2 but the error was large, while the branching ratio of $p2$ was consistent with 2.

On the f_2 fine structure at the L_1 edge, there are two prominent peaks at $\Delta E = 12.2^{+1.1}_{-0.9}$ eV and $\Delta E = 42.0^{+2.3}_{-3.3}$ eV. The prominent lines are clearly seen in the μ of iridium the L_1 edge in the Materials Data Repository. Although Sham[21] studied the L_1-edge x-ray absorption properties of 4d noble metals, there were two clear peaks of absorption coefficient at about 18 and 40 eV from the L_1 edge in Fig. 8 of Sham,[21] and these two peaks were associated with $2\ s \rightarrow p$, pd and $2\ s \rightarrow f$, respectively. This assignment of the two peaks will be helpful to consider the $p1$ and $p2$ assignments found in the iridium L_1 edge, although we cannot eliminate the possibility that $p2$ might be similar to extended XAFS (EXAFS) due to the large line width of 11^{+6}_{-6} eV.

3.3 *Ratio of the Scattering Factor* f_2 *Between* L_2 *and* L_3*-Edges*

The measured step size, which presents the depth of an edge, of the L_3 edge was twice that of the L_2 edge. Since the step-like edge features are associated with the $2p \rightarrow$ continuum transition, the ratio of the step size reflects the ratio, which is 1:2, of the initial core-electron states available for the L_2 ($2p_{1/2}$) and $L3$ ($2p_{3/2}$) processes. On the other hand, the WL, which is associated with $2p \rightarrow 5d$ transition, has a branching ratio $(L_3/L_2) > 2$. We investigated how the ratio of the scattering factor f_2 (L_3/L_2) changes with energy offset from WL.

At first, we estimated a floor value of f_2 in the energy region of ΔE from -100 to -50 eV, and then subtracted the floor value from the measured f_2. Next, the measured f_2 was smoothed by applying savgol_filter in python 3.8.2 with a window length of 5 and an order of 2 to reduce scattering of the ratio due to poor statistics. Figure 3 shows the f_2 after subtraction of the floor value and the ratio of $f_{2,L3}/f_{2,L2}$, where $f_{2,L3}$ and $f_{2,L2}$ are the f_2 at L_3 edge and L_2 edge, respectively. The solid line indicates the smoothed curve with savgol_filter. The energy $\Delta E'$ is the energy from the center energy of WL, because the uncertainty of the edge energy in our fitting results makes a discrepancy of the energy ΔE between L_2 and L_3 regions, and then the discrepancy makes pseudo peaks in the ratio near WL. A typical 1σ error of the ratio at the energy $\Delta E' > 0$ is 0.14.

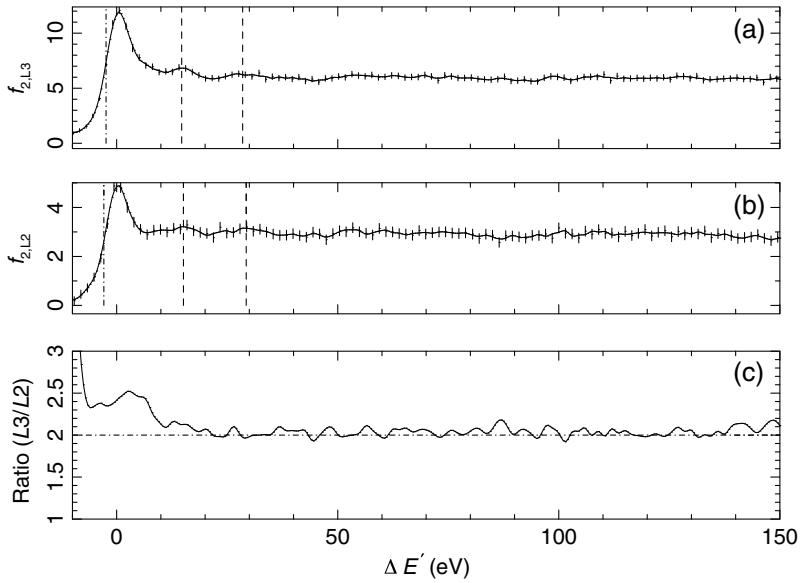

Fig. 3 Ratio of the atomic scattering factor f_2 between L_3 and L_2. $\Delta E'$ is the energy from WL. (a) and (b) The solid lines show the values after smoothing, the dashed lines indicate the energy of *p*1 and *p*2 features, and the dashed-dotted lines indicate the *L*-edge energy.

The branching ratio around the energy of WL is about 2.4, which is significantly >2. The branching ratio remains large up to $\Delta E' \sim 7.5$ eV. This result is consistent with a larger line width of WL in L_3 than that in L_2. In the energy region $\Delta E' = 8$ to 18 eV, the ratio is 2.1–2.2, which is slightly larger than 2. This result is also in agreement with the estimation of the results of the branching ratio of $p1$. Above 20 eV, the branching ratio becomes to be a mean value of 2.04 with a standard deviation of 0.05, which is consistent with the ratio of the density of states between $2p_{1/2}$ and $2p_{3/2}$.

3.4 *Fine Structures at* ΔE *>50 eV Seen in the Scattering Factor* f_2

It is found that the f_2 structure of the L_3 data at $\Delta E > 50$ eV is similar to that of the L_2 data (see Fig. 2). The similarity can also be seen in the constant ratio of $f_{2,L3}/f_{2,L2}$ at $\Delta E > 20$ eV (see Fig. 4). The origin of the fine structure in EXAFS is the interference between the incoming and

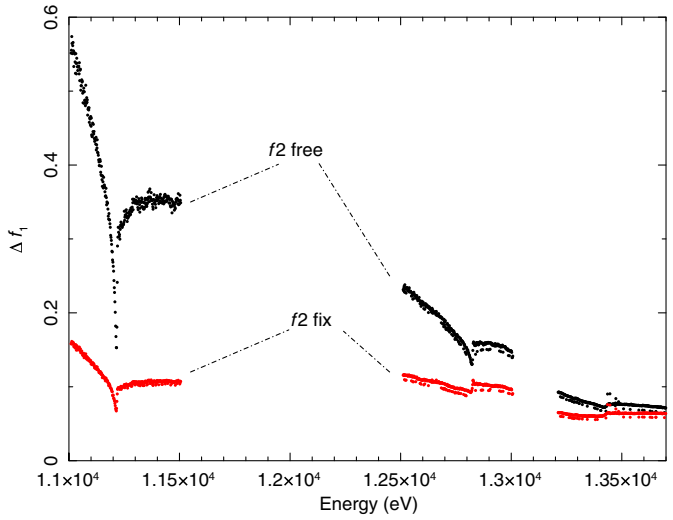

Fig. 4 Prediction of reducing the error in f_1 value using the f_2 estimated from μ. As a small error in μ was expected, f_2 was fixed on the best-fit value.

scattered photoelectron waves. The kinetic energy of a photoelectron wave is given by $E_K = h\nu - E_{\mathrm{edge}}$, where $h\nu$ is the photon energy and E_{edge} is the edge energy. Interference patterns should depend on E_K because the wavelength of a photoelectron is related to $1/E_K$. Thus, the fine structure in EXAFS of L_3 is expected to be similar to that of L_2.

We supposed that the fine structure of the L_1 data is also similar to that of the L_3 data, but we did not see a clear similarity. If we shift the energy of the $L_1 f_2$ data by $+20$ eV, we may see a weak similarity between the f_2 fine structures of L_3 and L_1.

4 Discussion

4.1 *Measurement of the Atomic Scattering Factors*

We have demonstrated that the f_2 fine structure obtained from the reflectance is similar to the XANES results obtained using XAS. This confirms the relationship between f_2 and μ and shows that f_2 can be estimated from μ. Estimating f_2 from μ may lead to reducing the time for the ground calibration of an x-ray mirror because the detailed structure of f_2 near the absorption edge is measured without a fine energy scan of the reflectance. In addition, because μ is accurately determined via XAS, the error margin in f_1 value obtained using μ is small. We demonstrate this possibility by fixing f_2 in our data. Figure 4 shows the error of f_1 when f_2 was fixed. It is found that the error in the f_1 value decreased by 0.3 to 0.8 times. As the critical angle for iridium at 12 keV is $\sim$0.385 deg, the x-ray reflectivity at an incident angle of 0.4 deg at an energy of 12 keV or less is not sufficiently low (Fig. 1). Thus, the uncertainty in the f_1 value is large when f_2 is set to a free parameter. Using μ may be worthwhile when using data wherein the incident angles are close to or below the critical angle.

4.2 *XAFS Measurement*

Our result suggests that the 10-nm-thick iridium formed by the DC magnetron sputtering device has almost the same optical property as that of iridium powder. This result indicates that a study of XAFS is possible with a thin layer instead of powder.

The reflectance measurements will be useful for fine structure research on thin atomic layer samples that are difficult to do with XAS technique. For thin films, the absorption coefficient is estimated by measuring the intensity of a fluorescence line (fluorescence XAFS measurements[22,23]). However, the self-absorption effect causes distortion in the measured spectra in fluorescence line, and a correction for this distortion is needed.[22] In addition, a sufficient intensity of fluorescence line is required to obtain μ with a high signal-to-noise ratio. Our reflectance measurement is an alternative method to estimate the absorption coefficient. The similarity between f_2 and μ suggests that the effects observed in the fluorescence XAFS measurements are small.

We have provided the fine structures of f_2 in the energy region $\Delta E < 50$ eV from iridium L-edges (L_3, L_2, and L_1). The properties of the two peaks are similar to those of $4d$ material obtained by Sham 1985. We have also calculated the ratio $f_{2,L3}/f_{2,L2}$ in the energy range $\Delta E' = 0 \sim 150$ eV. The ratio is about 2.4 in the energy range $\Delta E' < 7.5$ eV, and as the photon energy increases, the ratio decreases; at the energy $\Delta E' > 20$ eV, the ratio comes to the mean value of $\sim$2, which is consistent with the ratio of the density of states between $2p_{1/2}$ and $2p_{3/2}$.

The origin of the fine structure in EXAFS is the interference between the incoming and scattered photoelectron waves. Thus, each fine structure in the EXAFS region can be compared because we obtained the f_2 fine structures of the L-edges (L_3, L_2, and L_1). The f_2 fine structure of L_2 is, as expected, similar to that of L_3, but the f_2 fine structure of L_1 is not similar to that of L_3. If we shift the energy of the $L_1 f_2$ data by $+20$ eV, we may see a weak similarity between the f_2 fine structures of L_3 and L_1. This shift may be because of the difference between the L_1 transition ($\rightarrow 6p$) and the L_2/L_3 transition ($\rightarrow 5d$). Detailed analysis using high quality data is required to investigate the fine structures of iridium L-edges.

5 Conclusion

We measured the reflectance of an SPO plate coated with an iridium layer having a thickness of 10 nm at Spring-8 in the energy range covering all iridium L-edges.

We have shown that the shape of the fine structures of f_2 near L_2 and L_3 edges are remarkably similar to those in previous works on XAFS. The similarity suggests that we could obtain f_2 for a reflector substrate with an Ir film with a thickness of 10 nm by measuring the reflectance. In measuring the fine structure of the metal on the reflective surface at the fine energy pitch, the method used in this study leads to a reduction in the time of the ground calibration. Moreover, as the value of μ is well determined via XAS, the error in f_1 is reduced using f_2 estimated based on μ.

By comparing f_2 of L_3, L_2, and L_1, the ratio of f_2 values corresponding to L_3 and L_2 was found close to 2 and exceeded 2 near WL. Regarding the structure of XAFS, L_3 and L_2 are similar, and the energy apparently shifts between L_3 and L_1. This is probably because the final state of the transition is $5d$ for L_3 and L_2, whereas it is $6p$ for L_1. Further detailed analyses of the fine structures using an analysis tool such as Demeter 0.9.26 are therefore required.[24]

Acknowledgments

The X-ray measurement was performed at BL20B2 in SPring-8 with the approval of the Japan Synchrotron Radiation Research Institute (JASRI) (Proposal No. 2018B1106 (YM)). We used the MINUIT software package developed by CERN for the fitting procedure. This work was financially supported by JSPS KAKENHI [Grant Nos. 20H00175 (HM) and 21K18152(HA)]. We would like to thank Editage for English language editing. The authors have no relevant financial interests in the manuscript and no other potential conflicts of interest to disclose.

References

1. J. P. Clancy et al., "Spin-orbit coupling in iridium-based 5*d* compounds probed by x-ray absorption spectroscopy," *Phys. Rev. B* **86**, 195131 (2012).
2. T. Anniyev et al., "Complementarity between high-energy photoelectron and L-edge spectroscopy for probing the electronic structure of 5*d* transition metal catalysts," *Phys. Chem. Chem. Phys.* **12**, 5694–5700 (2010).
3. A. Wach, J. Sá, and J. Szlachetkoa, "Comparative study of the around-Fermi electronic structure of 5*d* metals and metal-oxides by means of high-resolution X-ray emission and absorption spectroscopies," *J. Synchrotron. Radiat.* **27**, 689–694 (2020).
4. H. Stragier et al., "Diffraction anomalous fine structure: a new x-ray structural technique," *Phys. Rev. Lett.* **69**, 3064 (1992).
5. I. Pickering et al., "Diffraction anomalous fine structure: a new technique for probing local atomic environment," *J. Am. Chem. Soc.* **115**, 6302 (1993)
6. B. L. Henke, E. M. Gullikson, and J. C. Davis, "X-ray interactions: photoabsorption, scattering, transmission, and reflection at E=50−30000 eV, Z=1–92," *At. Data Nucl. Data. Table* **54**(2), 181–342 (1993).
7. N. Kikuchi et al., "Atomic scattering factor of the ASTRO-H (Hitomi) SXT reflector around the gold's L edges," *Opt. Exp.*, **24**, 25548 (2016).
8. D. E. Graessle, et al. "Iridium optical constants for the Chandra X-ray Observatory from reflectance measurements of 0.05–12 keV," *Proc. SPIE* **5165**, 469 (2004).
9. H. Awaki, et al., "Measuring the atomic scattering factors near the iridium L-edges for the Athena silicon pore optics reflector," *J. Astron. Telesc. Instrum. Syst.* **7**, 014001 (2021).
10. R. L. Kelley et al., "The astro-H high resolution soft x-ray spectrometer," *Proc. SPIE* **9905**, 99050V (2016).
11. D. Barret et al. "The ATHENA X-ray integral field unit (X-IFU)," *Proc. SPIE* **10699**, 106991G (2018).
12. M. J. Collon, et al., "Silicon pore optics development for ATHENA," *Proc. SPIE* **9603**, 96030K (2015).

13. S. Massahi et al., "Installation and commissioning of the silicon pore optics coating facility for the ATHENA mission," *Proc. SPIE* **11119**, 111190F (2019).
14. S. Goto et al., "Construction and commissioning of a 215-m-long beamline at SPring-8," *Nucl. Instrum. Methods A* **467**, 682–685 (2001).
15. M. Yabashi, et al., "SPring-8 standard x-ray monochromators," *Proc. SPIE* **3773**, 2–13 (1999).
16. L. Nevot and P. Croce, "Caractérisation des surfaces par réflexion rasante de rayons X. Application à l'ètude du polissage de quelques verres silicates," *Rev. Phys. Appl.* **15**(3), 761–779 (1980).
17. S. Massahi et al., "Investigation of boron carbide and iridium thin films, an enabling technology for future x-ray telescopes," *Appl. Opt.* **59**, 10902–10911 (2020)
18. J. H. Sinfelt and G. D. Meitzner, "X-ray absorption edge studies of the electronic structure of metal catalysts," *Acc. Chem. Res.* **26**(1), 1–6 (1993).
19. J. A. Horsley, "Relationship between the area of $L_{2,3}$ x-ray absorption edge resonances and the d orbital occupancy in compounds of platinum and iridium," *J. Chem. Phys.* **76**, 1451 (1982).
20. V. Monteseguro et al., "Phase stability and electronic structure of iridium metal at the megabar range," *Sci. Rep.* **9**, 8940 (2019).
21. T. K. Sham, "L-edge x-ray-absorption systematics of the noble metals Rh, Pd, and Ag and the main-group metals In and Sn: a study of the unoccupied density of states in 4D elements," *Phys. Rev. B.* **31**, 1888–1902 (1985).
22. M. Honda et al., "A fluorescence XAFS measurement instrument in the soft x-ray region toward observation under operando conditions," *Rev. Sci. Instrum.* **86**, 035103 (2015).
23. L. Tröger et al., "Full correction of the self-absorption in soft-fluorescence extended x-ray-absorption fine structure," *Phys. Rev. B*, **46**, 3283 (1992).
24. B. Ravel and M. Newville, "ATHENA, ARTEMIS, HEPHAESTUS: data analysis for X-ray absorption spectroscopy using IFEFFIT," *J. Synchrotron Radiation* **12**, 537–541 (2005).

Biographies of the authors are not available.